the formula $C_{91}H_{158}N_{23}O_{24}$ and crystallizes in space group $C222_1$ with $Z = 8$. There are 138 non-hydrogen atoms in the asymmetric unit and the data extend to 0·8Å resolution. Exhaustive trials with various direct-methods techniques were unsuccessful. The weighting scheme was used for both triplets and negative quartets; magic-integer phase permutation was used with 11 reflections in the starting set. A total of 640 phase sets was generated, and the best solution yielded an E map in which 52 atoms were clearly visible. The structure was completed by standard Fourier techniques.

The filtering of very low-order reflections is, in general, much less successful, largely because we are trying to encourage direct methods to build a molecular shape as early as possible. However, in the case of WINTER2 (Table 1), removing all reflections with $(\sin^2\theta)/\lambda^2 < 0{\cdot}016$ produced an E map in which 50 out of 88 non-hydrogen atoms were located. It is worth noting that this is the only structure tested that has a disordered solvent of appreciable scattering power. This type of filter could be of general applicability in these circumstances.

4. Concluding remarks

This method is simple to apply and can be very effective. It requires no extra computing time except in cases when the scheme filters so many reflections that the convergence map becomes fragmented with many gaps. In these circumstances a larger starting set is necessary with a corresponding increase in computer time. There is no clear distinction between the efficacy of the weighting scheme or the cut-off method - sometimes one technique works and sometimes the other, as is the nature of direct methods. Because of the small associated overheads, we recommend this technique as a routine option to be used in cases of difficulty.

References

BUTTERS, T., HÜTTER, P., JUNG, G., PAULS, P., SCHMITT, H., SHELDRICK, G. M. & WINTER, W. (1981). *Angew. Chem.* **93**, 904-905.

CASCARANO, G., GIACOVAZZO, G., CAMALLI, M., SPAGNA, R., BURLA, M. C., NUNZI, A. & POLIDORI, G. (1984). *Acta Cryst.* A**40**, 278-283.

COLENS, A., DECLERCQ, J. P., GERMAIN, G., PUTZEYS, J. P. & VAN MEERSSCHE, M. (1974). *Cryst. Struct. Commun.* **3**, 119-122.

DETITTA, G. T., LANGS, D. A., EDMONDS, J. W. & DUAX, W. L. (1980). *Acta Cryst.* B**36**, 638-645.

GIACOVAZZO, C. (1976). *Acta Cryst.* A**32**, 967-976.

GIACOVAZZO, C. (1977). *Acta Cryst.* A**33**, 527-531.

GILMORE, C. J. (1984). *J. Appl. Cryst.* **17**, 42-46.

GILMORE, C. J. & HAUPTMAN, H. A. (1985). *Acta Cryst.* A**41**, 457-462.

HAUPTMAN, H. A. (1972). *Crystal Structure Analysis: the Role of the Cosine Seminvariants.* New York: Plenum Press.

HAUPTMAN, H. A. (1985). *Acta Cryst.* A**41**, 454-456.

IRNGARTINGER, H., REIBEL, W. R. K. & SHELDRICK, G. M. (1981). *Acta Cryst.* B**34**, 1387-1389.

KARLE, I. L. (1975). *J. Am. Chem. Soc.* **97**, 4379-4386.

KARLE, J. (1979). *Proc. Natl Acad. Sci. USA*, **76**, 2089-2093.

KARLE, J. (1980). *Proc. Natl Acad. Sci. USA*, **77**, 5-9.

KARLE, J. & HAUPTMAN, H. A. (1953). *Acta Cryst.* **6**, 473-476.

MESSAGER, J. C. & TSOUCARIS, G. (1972). *Acta Cryst.* A**28**, 482-484.

SCHENK, H. (1973). *Acta Cryst.* A**29**, 77-82.

SHELDRICK, G. M., DAVISON, B. E. & TROTTER, J. (1978). *Acta Cryst.* B**34**, 1387-1389.

SHELDRICK, G. M. & TROTTER, J. (1978). *Acta Cryst.* B**34**, 3122-3124.

SUCK, D., MANOR, P. C. & SAENGER, W. (1976). *Acta Cryst.* B**32**, 1727-1735.

VITERBO, D. & WOOLFSON, M. M. (1973). *Acta Cryst.* A**29**, 205-208.

WILSON, A. J. C. (1949). *Acta Cryst.* **2**, 318-321.

Acta Cryst. (1988). A**44**, 1021-1028

Analytical X-ray Line Profile Analysis Based Upon Correlated Dislocations

BY SATISH RAO AND C. R. HOUSKA

Department of Materials Engineering, Virginia Polytechnic Institute and State University, Blacksburg, VA 24061, *USA*

(*Received* 8 *February* 1988; *accepted* 31 *May* 1988)

Abstract

Recent advances describing X-ray line profiles analytically, in terms of a minimum number of parameters, are related to a theory based upon correlated dislocations. It is shown that a multiple convolution approach, based upon the Warren-Averbach (W-A) analysis, leads to a form that closely approximates the strain coefficient obtained by Krivoglaz, Martynenko & Ryaboshopka [*Phys. Met. Metall.* (1983), **55**, 1-12]. This connection enables one to determine the dislocation density and the ratio of the correlation range parameter to the mean particle size. These two results are obtained most accurately from previous analytical approaches which make use of a statistical least-squares analysis. The W-A Fourier-

0108-7673/88/061021-08$03.00

series approach provides redundant information and does not focus on the critical parameters that relate to dislocation theory. Results so far are limited to b.c.c. materials. Results for cold-worked W, Mo, Nb, Cr and V are compared with highly imperfect sputtered films of Mo. A major difference is relatable to higher correlation of dislocations in cold-worked metals than is found in sputtered films deposited at low temperatures. However, in each case, the dislocation density is high.

1. Introduction

The analysis of X-ray diffraction line shapes using the Warren & Averbach (W-A) theory (Warren, 1959), was initially developed with the goal of obtaining experimental results with a minimum of *a priori* assumptions. Its popularity and existence dating back to the 1950's have resulted in a vast accumulation of data which has long since allowed those few assumptions inherent in the development to be examined critically. It has been recognized that the expansion of strain terms in this development must involve small quantities or else the strains should be describable by a Gaussian distribution. If the latter is true, the strain term becomes rigorous. The latter appears to have experimental validity at least over a limited range of those crystal distances that dominate the shape of a diffraction peak.

The results obtained from the W-A analysis are limited to particle size and strain, which do not relate directly to dislocation theory. Several papers have attempted to fill this gap. However, the treatment of displacements from dislocation fields presents difficulties and requires simplifying assumptions if useful results are to be obtained. Wilkens (1970) has developed an expression involving the dislocation density n_d and a cut-off radius which appears to provide a description of certain profiles. The use of a cut-off radius places a limit on the range of the distortion field. More recently, Krivoglaz, Martynenko & Ryaboshopka (1983) have added to the dislocation approach by introducing correlation between dislocations within each parallel array. This development resulted in the introduction of a screening parameter R_c which determines the rate at which the dislocation pair probability falls off with distance. The problem of accounting for the interactions between non-parallel arrays has not been treated. However, this treatment appears to be the most highly developed approach and deserves a critical quantitative examination in terms of reliable line profile data.

Houska & Smith (1981) eliminated the need for fitting profiles by means of the usual Fourier transform, and instead developed a statistical analytical fitting procedure. This was later extended into an exact analytical expression by Rao & Houska (1986*b*), who found excellent numerical agreement with the prior development. Either approach provides a statistical fit of line profile data which allows a confidence level to be assessed for the critical parameters, *i.e.* two root mean square strain parameters and particle size. The analytical functions allow profiles to be constructed without troublesome termination errors and the associated oscillations that are found in synthesizing the Fourier series after applying the Stokes correction. This can be a serious problem when one encounters overlapping profiles typically found in powder patterns.

Our primary goal is to link the most recent dislocation field approach, based upon correlated dislocations, with our statistical-analytical (S-A) approaches. This ultimately provides the degree of pair correlation between dislocations and their density. Examples are given using existing data from b.c.c. cold-worked metals, and imperfect sputtered films containing a high density of dislocations.

2. Theory

Line shapes from statistical treatment

The shape of a diffraction line can be described by

$$P'(h_3) = Y_0\left[1+2\sum_{n=1}^{\infty} A_n \cos\left[2\pi n(h_3-l)\right]\right], \quad (1)$$

where h_3 is the usual reciprocal-space variable given by $h_3 = 2\langle d\rangle \sin\theta/\lambda$, $\langle d\rangle$ is the average interplanar spacing for (001) planes, $L = n\langle d\rangle$ is a column distance, θ is the angle of incidence and scattering, λ is the wavelength, and Y_0 is a scaling constant.

The overall Fourier coefficient is given by

$$A_n = (A_C^L)^n (A_G^L)^{n^2} A_n^S (A_I^D)^n (A_I^U)^{n^2} \quad (2)$$

with

$$(A_I^D)^n = [\exp(-2\pi^2\langle\varepsilon_{1D}^2\rangle l^2)]^n \quad (3a)$$

$$(A_I^U)^{n^2} = [\exp(-2\pi^2\langle\varepsilon_{1U}^2\rangle l^2)]^{n^2}. \quad (3b)$$

A mean-square strain $\langle\varepsilon_{1D}^2\rangle$ parameter is relatable to Cauchy-like profiles and $\langle\varepsilon_{1U}^2\rangle$ to Gaussian-like profiles.

The particle size coefficient, based upon coherent spherical regions, is given by

$$A_n^S = 1 - n/N_3 + (4/27)(n/N_3)^3, \quad n < \tfrac{3}{2}N_3, \quad (4a)$$

$$A_n^S = 0, \quad n > \tfrac{3}{2}N_3, \quad (4b)$$

where N_3 is the average number of unit cells per column. The first two terms in (4*a*) represent the fraction of nth neighbors for columns of height N_3. The cubic term allows for the distribution of heights within a sphere of diameter $\frac{3}{2}N_3$. As in W-A theory, we assume that within a coherent region or particle the boundary is well defined or discrete. That is, a pair of atoms is either inside or outside the coherent region. This cut-off becomes less clear for a

distribution of nearly random dislocations in a crystal without boundaries.

The first of the instrumental coefficients is relatable to a pure Cauchy profile and is defined by

$$A_C^I = \exp(-2\pi a_\gamma), \tag{5a}$$

where a_γ represents a shape-fitting parameter. The corresponding Gaussian coefficient is

$$A_G^I = \exp(-\pi a_\beta^2). \tag{5b}$$

By multiplying Fourier coefficients according to (2), the strain, particle size, and instrumental contributions become convoluted to provide a line profile that can be directly related to experimental results.

Equation (1) is written more conveniently as an integral.

$$\frac{P'(h_3^0)}{2N_3Y_0} = \int_0^{3/2} [1 - u + \tfrac{4}{27}u^3] \times \exp[-(\gamma u + \beta u^2)] \cos 2\pi h_3^0 u \, du, \tag{6}$$

with

$$u = n/N_3, \qquad h_3^0 = N_3 h_3, \tag{7a}$$

$$\gamma = 2\pi N_3(a_\gamma + \pi\langle\varepsilon_{1D}^2\rangle l^2) \tag{7b}$$

and

$$\beta = \pi N_3^2(a_\beta^2 + 2\pi\langle\varepsilon_{1U}^2\rangle l^2). \tag{7c}$$

All parameters contributing toward a Cauchy profile are located in γ while those that are Gaussian are found in β. The parameters a_γ and a_β are obtainable from profiles that contain only instrumented broadening. As was stated previously, (6) has been evaluated in two ways which give nearly identical numerical results. These analytical forms enable one to carry out a least-squares fit of the measured profiles. Also, the construction of misfit surfaces enables one to establish confidence levels for both strain and particle size parameters. The latter is not readily carried out from the lengthy Fourier series described by (1).

Strain information is expressed in terms of mean square strain for different distances $n\langle d\rangle$ along directions normal to the reflecting planes. This has been simplified to

$$\langle\varepsilon_n^2\rangle = (1/n)\langle\varepsilon_{1D}^2\rangle + \langle\varepsilon_{1U}^2\rangle \tag{8}$$

for those distances that influence a Bragg profile. The profile is largely shaped by the relative displacements of pairs of cells within the range

$$N_3/10 < n < N_3. \tag{9}$$

The parameters $\langle\varepsilon_{1D}^2\rangle$ and $\langle\varepsilon_{1U}^2\rangle$ allow $\langle\varepsilon_n^2\rangle$ to be evaluated over this limited range.

Equation (8) presents the results in a purely statistical form and does not provide a basic connection with dislocation fields. The connection is made later by using a Fourier coefficient of the form

$$A_L = \left[1 - \frac{L}{\langle L\rangle} + \frac{4}{27}\left(\frac{L}{\langle L\rangle}\right)^3\right] \times \exp[(-C_1 L + C_2 L^2)l^2] \tag{10}$$

with

$$C_1 = 2\pi^2\langle\varepsilon_{1D}^2\rangle/\langle d\rangle$$

$$C_2 = 2\pi^2\langle\varepsilon_{1U}^2\rangle/\langle d\rangle^2.$$

Note that $\langle d\rangle$ is the average spacing for the first order of a set of reflections $(h_1k_1l_1)\ldots(nh_1, nk_1, nl_1)$ and that this requires one index according to $(00l)$. The exponential term in (10) is the strain term, A_L^D, which will be treated in the next section.

Correlated dislocations

Krivoglaz *et al.* (1983) have simplified the calculation of column strain by considering a parallel array of correlated dislocations. One type of array will have parallel core orientations with Burgers vectors that are both parallel and antiparallel in equal numbers. Screw and edge arrays are treated separately. Although there are usually several distinguishable arrays, each is considered independently. The orientation of the core and Burgers vector are determined from crystallographic considerations, *i.e.* planes and lines of close packing.* Within one array, the average displacement for each pair of cells is determined by allowing individual dislocations as well as correlated pairs to take on all parallel positions consistent with three long-range distribution functions. The final Fourier coefficient is determined by averaging the cell displacements over crystallographically distinguishable arrays with equal probability for both screw and edge types.

Pair probabilities $\varepsilon_{\alpha\alpha'}$ are defined relative to a random distribution according to

$$\varepsilon_{\alpha\alpha'} = P_{\alpha\alpha'}(r) - C_\alpha C_{\alpha'}. \tag{11}$$

Here α designates both the core and Burgers vector for one member of a pair, while α' designates a second parallel dislocation at a radial vector distance r but with an antiparallel Burgers vector. C_α = probability of finding one type of dislocation α in a given position. With a Gaussian pair probability, $\varepsilon(r)$ is given by

$$\varepsilon(r) = (C\Delta/4\pi R_C^2)\exp(-r^2/R_c^2) \tag{12}$$

with $C = C_\alpha + C_{\alpha'}$, where we note that $C_\alpha = C_{\alpha'}$. The total probability C is related to the dislocation density by $n_d = C/\Delta$, with Δ = area per atom on planes perpendicular to the dislocation cores [*i.e.* (111) for b.c.c.].

* For example in b.c.c. materials there are four arrays for screw dislocations and 12 arrays for the edge dislocation.

One finds that the distribution is long range and best scaled in units of $\langle L\rangle$. An additional and important condition for a cylindrical array requires

$$2\pi \int \varepsilon(r) r \, dr = C\Delta/4. \tag{13}$$

This requirement causes the long-range displacement term to go to zero making the results independent of the shape of the crystal and the nature of the distribution of stress on its surface.

These basic guidelines lead one to the following result for the exponent of the strain coefficient.

$$A_L^D = e^{-T} \tag{14a}$$

with

$$-T = K(\pi R_c^2 n_d) l^2 (X^2 \ln X) \tag{14b}$$

$$K = \tfrac{1}{2}\langle\chi\rangle (b/\langle d\rangle)^2 (\langle\xi\rangle/\xi')^2$$

$$X = (\xi'/\langle\xi\rangle) L/R_c$$

and

$$\xi' = 1{\cdot}344.$$

We have rearranged terms and defined a variable X which is convenient in the analysis. Quantities appearing in K will be defined in the following discussions dealing with b.c.c. materials. χ depends upon the orientation of the dislocation and its Burgers vector relative to the diffraction vector $\mathbf{S}_\lambda$. The result obtained for one array of screw dislocations is

$$\chi_S = \sin^2\psi \cos^2\psi \tag{15}$$

and for the edge

$$\chi_E = [1 - 4\nu + 8\nu^2 + 4(1-2\nu)\sin^2\varphi] \times \sin^4\psi/[8(1-\nu)^2] \tag{16}$$

where ν = Poisson's ratio.

The angles φ and ψ are defined in Figs. 1(a) and (b). For screw dislocations, the maximum cell displacements occur for columns oriented at $\psi = 45°$; while for pure edge dislocations, the maximum occurs when the core is perpendicular to $\mathbf{S}_\lambda$ and parallel to the Burgers vector. Because several equivalent crystallographic directions are possible, an average is taken over all arrays. If these have equal probability, one obtains

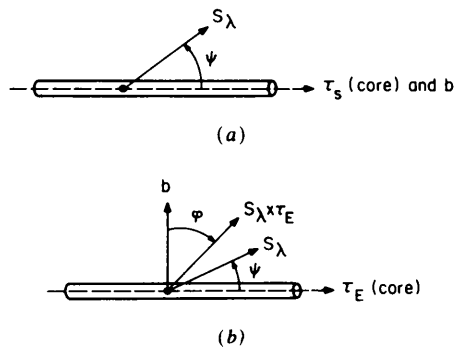

Fig. 1. Pictorial definition of angles φ and ψ found in equations (15) and (16), for (a) screw and (b) edge dislocations.

Table 1. *Separate listings of average* $\langle\chi\rangle$ *and* $\langle\xi\rangle$ *for screw* (S), *edge* (E) *and the weighted average over edge and screw* (SE)

hkl	l_0^2	$\langle\chi_S\rangle$	$\langle\chi_E\rangle$	$\langle\chi_{SE}\rangle$	$\langle\xi_S\rangle$	$\langle\xi_E\rangle$	$\langle\xi_{SE}\rangle$
110	2	0·111	0·184	0·166	3·46	2·17	2·37
200	4	0·222	0·155	0·172	2·45	2·33	2·39
211	6	0·111	0·184	0·166	2·71	1·97	2·08
220	8	0·111	0·184	0·166	2·87	1·80	1·97
301	10	0·182	0·164	0·169	2·34	1·98	2·06
Averages over *hkl*				0·168			2·174

$$\langle\chi_S\rangle = \tfrac{2}{9}[1 - 2\Gamma(hkl)] \tag{17}$$

for screw and

$$\langle\chi_E\rangle = [144(1-\nu)^2]^{-1} \times [25 - 68\nu + 72\nu^2 + (19 - 44\nu + 24\nu^2)\Gamma] \tag{18}$$

for edge with

$$\Gamma = \frac{h^2k^2 + k^2l^2 + l^2h^2}{(h^2 + k^2 + l^2)^2}. \tag{19}$$

Since there are three times as many arrays of edge dislocations as screw in the b.c.c. the weighted average over both types is

$$\langle\chi_{SE}\rangle = \tfrac{3}{4}\langle\chi_E\rangle + \tfrac{1}{4}\langle\chi_S\rangle. \tag{20}$$

Individual values of χ are listed in Table 1 for W and Mo and vary with *hkl* over this limited range. This variation is well within any experimental errors encountered in line shape analyses. If one examines variations due to Poisson ratio for other b.c.c. materials, one finds about 10% change in $\langle\chi_{SE}\rangle$ which is within the limitations of both theory and the data when taken equal to 0·168.

The quantity $\langle\xi\rangle$ appears not only in K but also in the variable X. It is obtained by taking an average for all dislocation arrays with respect to each column direction, *i.e.* [110], [200] *etc.* For one orientation of screw dislocation array, this has been defined as*

$$\ln\xi = \ln 2 - \ln|\sin\psi|, \qquad p = 1 \tag{21}$$

$$\ln\xi = 1{\cdot}116 - \ln|\sin\psi| - \ln p + 1/3p^2, \qquad p > 1. \tag{22}$$

For a random positioning of dislocations onto planes and directions of highest packing, $\langle\xi\rangle$ depends purely upon crystallographic considerations and p. The latter is given by

$$p = \mathbf{S}_\lambda \cdot \mathbf{b} \tag{23}$$

* Equations (21) and (22) were first applied to edge dislocations by Wilkens (1970). Calculations for $\langle\xi_{SE}\rangle$, as given in Table 1, were carried out on this basis.

Table 2. *Listing of* $\langle \xi'' \chi^2 \rangle$ *for* W *and* Mo

hkl	l_0^2	$\langle \xi'' \chi^2 \rangle$
110	2	0·0095
200	4	0·0072
211	6	0·0253
220	8	0·0262
310	10	0·0185

with the magnitude of the diffraction vector in reciprocal space given by $|\mathbf{S}_\lambda| = l/\langle d \rangle$. Table 1 provides a listing of five low-order peaks that are normally in a range where (14*b*) is applicable for b.c.c. materials. For this restricted listing, one finds about a ±10% variation of $\langle \xi \rangle$ with *hkl* after averaging over both screw and edge arrays. Therefore, we treat it as a constant equal to 2·174.

With n_d representing the number of dislocations per unit area, the product $(\pi R_c^2 n_d)$ is the number of dislocations in a circular range of radius R_c. Both screw and edge with all orientations are considered.

The correction term

$$\delta T_1(L) = 2(\pi R_c^2 n_d)\left[\frac{b}{\langle d \rangle}\right]^2 l^2 \left[\frac{\langle \xi \rangle}{\xi'}\right]^4 \langle \xi'' \chi^2 \rangle X^4 \quad (24)$$

to (14) has been fully evaluated only for screw dislocations. This contains terms already defined except for

$$\xi'' = \frac{1}{8}\left(-\frac{1}{2} + (-1)^p p + p^2 \left\{ \frac{7}{4} + [1 + (-1)^{p+1}] \ln 2 \right.\right.$$
$$- \tfrac{1}{2}[1 + (-1)^p] \sum_{k=1}^{p/2} \left[\frac{(-1)^k}{k} + \frac{2}{2k-1} \right]$$
$$\left.\left. - [1 + (-1)^{p+1}] \sum_{k=1}^{(p-1)/2} \frac{1}{2k-1} \right\} \right). \quad (25)$$

The average $\langle \xi'' \chi^2 \rangle$ is given in Table 2 for b.c.c. and those reflections appropriate to this approach. Without a comparable development for edge dislocations, (24) is useful primarily for estimating the maximum value of X over which (14*b*) is valid. Under these conditions, the fractional correction at X_m is approximately

$$\frac{\delta T_1}{T} = 4\left[\frac{\langle \xi \rangle}{\xi'}\right]^2 \frac{\langle \xi'' \chi^2 \rangle}{\langle \chi \rangle} \frac{X_m^2}{\ln X_m} \quad (26)$$

where $X_m = (\xi'/\langle \xi \rangle)(\langle L \rangle / R_c)$ and $\langle L \rangle = N_3 \langle d \rangle$. Fig. 2 illustrates the magnitude of (26) as a function of X_m for 220. We will return to this restriction on X_m when considering results for tungsten.

Relationships between analytical and correlated-dislocations theories

So far, there is a gap between the correlated-dislocation approach and the W-A approach. This is best closed by beginning with our analytical treatment. Sample information is contained in two strain parameters $\langle \varepsilon_{1D}^2 \rangle$ and $\langle \varepsilon_{1U}^2 \rangle$ and the average column height $\langle L \rangle$. These quantities may be simply related to the dislocation density and the range parameter R_C. The average column height is an additional parameter not explicitly considered in the dislocation approaches. Normally, we think of the average column height as the mean size of a subgrain having some boundary feature that sharply destroys the periodicity within a crystal. In heavily cold-worked metals, a well defined sharp interface may not exist. Instead, one might have a diffuse boundary extending over a range of interatomic distances that is not likely to be perfectly repetitive but, rather, statistical, having an irregular spacing. Krivoglaz *et al.* (1983) did not treat distributions that lead directly to such a particle size term. Perhaps the answer to the particle size question lies in a further development in the antiscreening model taken with an appropriate distribution function. The evidence for a separate particle size term is sufficiently convincing to proceed with this explicitly included in the profile analysis for either sharp or diffuse boundaries.

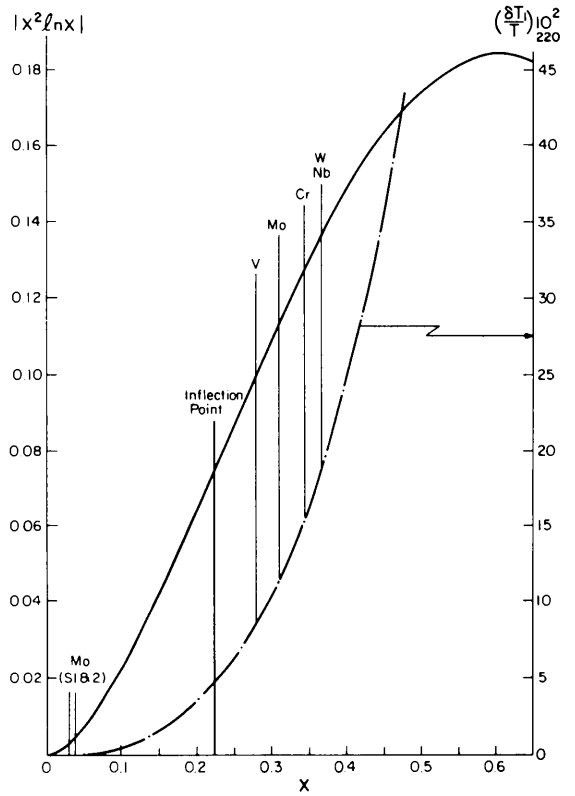

Fig. 2. Exponential shape function $X^2 \ln X$ found in Fourier coefficient and first-order correction for 220. Cluster locations of cold-worked filings and sputtered films relative to inflection point. References: W (McKeehan & Warren, 1953); Cr, Nb, V (Aqua & Wagner, 1964); Mo (Despujols & Warren, 1958); Mo (*S*1, *S*2) (Houska & Smith, 1981).

It can be shown that the function $X^2 \ln X$ in (14*b*) can be well represented by a power series up to the quadratic term. This has already been expressed in the exponential strain term as $C_1L+C_2L^2$ [(10)]. Here, the expansion is written in terms of the length L between pairs of cells along a column. An optimum least-squares fit gives the form

$$T' = \tfrac{1}{2}(\pi R_c^2 n_d) b^2 \left[\frac{\langle\xi\rangle}{\xi'}\right]^2 \langle\chi\rangle \left[\frac{l}{\langle d\rangle}\right]^2 \times [0{\cdot}620 X_m X - (\ln 1{\cdot}792 X_m) X^2] \quad (27)$$

with $X_m = (\xi'/\langle\xi\rangle)(\langle L\rangle/R_c)$. Figs. 3 and 4 illustrate fits for $X_m = 0{\cdot}03$ and 0·37 which are well within the error of a conventional W-A analysis.

If like terms are compared in (27) and in the equation

$$T_E = 2\pi^2 l^2 \left[\left(\frac{\langle\xi\rangle R_C}{\xi'\langle d\rangle}\right)\langle\varepsilon_{1D}^2\rangle X + \left(\frac{\langle\xi\rangle R_c}{\xi'\langle d\rangle}\right)^2 \langle\varepsilon_{1U}^2\rangle X^2\right] \quad (28)$$

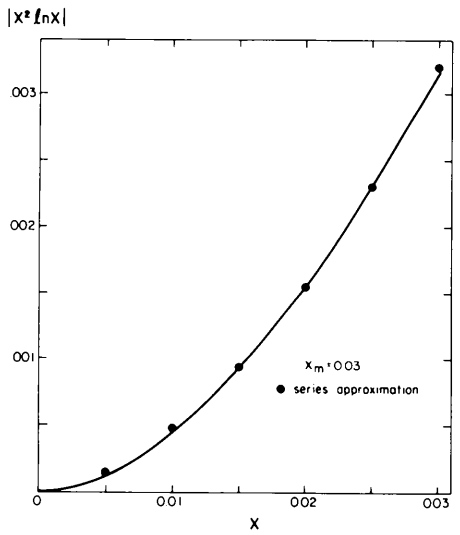

Fig. 3. Least-squares fit of $X^2 \ln X$ up to $X_m = 0{\cdot}03$, with a power series up to the quadratic term ($C_1X + C_2X^2$).

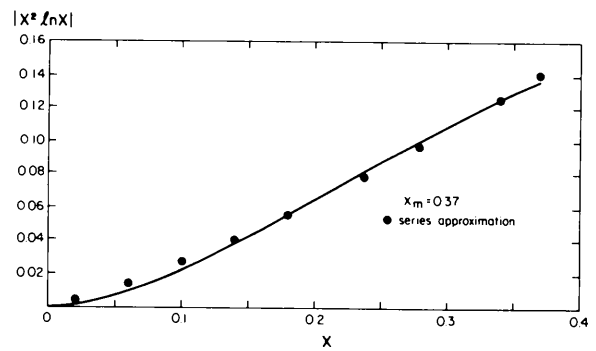

Fig. 4. Least-squares fit of $X^2 \ln X$ up to $X_m = 0{\cdot}37$, with a power series up to the quadratic term ($C_1X + C_2X^2$).

one finds that the dislocation density is given by

$$n_d = 20{\cdot}3 \frac{\langle d\rangle}{b^2\langle\chi\rangle} \frac{\langle\varepsilon_{1D}^2\rangle}{\langle L\rangle}. \quad (29)$$

This varies directly with the strain parameter and inversely with the mean particle size. Similarly, for a Gaussian distribution, one obtains

$$\frac{R_c}{\langle L\rangle} = 1{\cdot}10 \exp\left(0{\cdot}62 \frac{\langle L\rangle\langle\varepsilon_{1U}^2\rangle}{\langle d\rangle\langle\varepsilon_{1D}^2\rangle}\right). \quad (30)$$

The range R_c increases relative to $\langle L\rangle$ as the experimental quantities $\langle L\rangle$ and $\langle\varepsilon_{1U}^2\rangle/\langle\varepsilon_{1D}^2\rangle$ increase.

3. Applications of expanded analytical profile analysis

Calculations were carried out for several b.c.c. materials which include W, Mo, Nb, Cr and V. The most extensive data collection, for any one sample, is for the W data of McKeehan & Warren (1953), which offers a critical test. This is due largely to its elastic isotropy which enables data from different crystal directions to be interrelated as one data set. Molybdenum also provides interesting results because data from filings (Despujols & Warren, 1958) may be compared with those obtained from films by sputter deposition (Houska & Smith, 1981). In these cases, profiles from the 110 and 220 reflections have been studied with sufficient accuracy to provide meaningful results.

For the following reasons, care must be taken to ensure that data sets are examined within a restricted range of X values. First of all, corrections introduced by the second-order term (δT_1) should be kept to a small fraction of the first-order term T to conform safely with first-order theory. The maximum tolerated throughout the fitting procedure is 18% (see Fig. 2). The correction at $L = 160$ Å using tungsten data approaches this value. However, it is likely that the error in the distortion coefficient for $L/\langle L\rangle \geq 0{\cdot}8$, after making the Stokes correction and after separating Fourier coefficients, could be at or above the 18% level. A second consideration for restricting X is related to the power expansion given in (27). A re-examination of Fig. 4 shows that (27) provides an excellent approximation to (14*b*) for $X_m = 0{\cdot}37$. In fact, the series approximation remains good at least to $X_m = 0{\cdot}47$. With these considerations in mind, we truncate the W data at $L = 160$ Å or $L/\langle L\rangle = 0{\cdot}8$. X_m is about 0·030 for both sputter-deposited films which, of course, gives an excellent fit.

Calculations for $\langle\xi''\chi^2\rangle$, which appears in the second-order correction [(26)], revealed that this term more than doubles in going from the 310 to the 222 reflection. Therefore, taking $l_0^2 > 10$ becomes risky if one wishes to conform with the first-order theory. Accordingly, the data fits for the distortion

coefficients, A_L^D, have been truncated both in L and in *hkl*. Finally, the large displacements in the core region of a dislocation have not been included in the theory. Only the long-range purely elastic displacement fields are included. The latter play the major role in shaping those portions of profiles that can be measured accurately. Core-region displacements could cause problems in the separation procedure of the Fourier coefficients normally employed in the W-A analysis at the lowest L values. Because of these problems, values of L at and below 40 Å are discarded in the fitting procedure.

An examination of Fig. 5 shows that the fit to theory is good over 30 data points which encompass five *hkl* reflections. The parameters L, $\langle\varepsilon_{1D}^2\rangle$ and $\langle\varepsilon_{1U}^2\rangle$ giving this fit are listed in Table 3, along with six other b.c.c. materials. The extended tabulation of experimental data for elastically anisotropic materials is based upon the analyses of (110) and (220) planes using published data referenced in the caption. In all cases, L/R_c locates X_m at or below the 0·37 limit used for W. This may be seen in Fig. 2 as well as a clustering of data obtained from 'cold-worked' filings above $X_m = 0{\cdot}22$ (inflection point) and below for samples prepared by sputtering.

If one considers the difficulties in obtaining accurate values of A_L^D, the spread in $R_c/\langle L\rangle$ obtained from (30) for V, Mo, Cr and Nb (data from Aqua & Wagner, 1964) is not likely to be significant. However, differences in the dislocation densities n_d are more meaningful.

4. Discussion

Our results have demonstrated that the line shape theory as developed by Krivoglaz *et al.* (1983) and our previously developed analytical approaches are compatible and can explain profiles that vary continuously from a Cauchy-like to a Gaussian-like shape. The Cauchy-like shape may be related to highly clustered unlike dislocations while the Gaussian-like shapes relate to more random arrangements. In terms of the original W-A Fourier approach, the shape of a profile depends upon the way the mean square strain $\langle\varepsilon_L^2\rangle$ varies with distance. Linking this dependence with dislocation fields, having a prescribed correlation, provides a fundamental connection with basic theory. This extension to our analytical profile calculations relates the shapes of multiple orders from a set of (*hkl*) planes to the mean particle size, dislocation density and the correlation range.

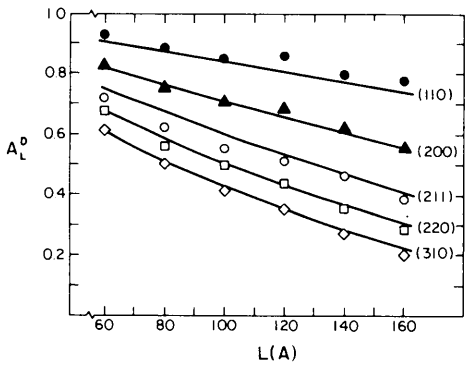

Fig. 5. Fit of experimental W strain coefficients (McKeehan & Warren, 1953) with correlated dislocation theory (Krivoglaz *et al.*, 1983).

Table 3. *Final results of extended line shape analysis giving X_m, n_d and $R_c/\langle L\rangle$ in terms of N_3, $\langle L\rangle$, $\langle\varepsilon_{1D}^2\rangle$ and $\langle\varepsilon_{1U}^2\rangle$ for seven b.c.c. samples*

	X_m	N_3	$\langle L$(Å)$\rangle$	$n_d \times 10^{11}$ (cm^{-2})	$R_c/\langle L\rangle$	$\langle\varepsilon_{1D}^2\rangle \times 10^4$	$\langle\varepsilon_{1U}^2\rangle \times 10^6$
Cr	0·274	140	285	3·67	1·79	2·63	1·47
V	0·226	93·7	200	6·56	2·17	3·46	4·05
Mo	0·246	117	260	4·60	1·99	3·30	2·72
W	0·368	89·4	200	1·53	1·33	0·84	0·29
Nb	0·295	92·1	215	7·32	1·66	4·56	3·27
Mo(*S*1)	0·030	83·6	186	0·92	16	1·88	9·61
Mo(*S*2)	0·022	397	884	0·17	22	1·69	2·04

If subgrain size broadening plays a significant role, even though dislocations may be highly clustered, the shapes will not be purely Cauchy. The exact shape will be influenced by the mean particle size and the variance of the size distribution (Rao & Houska, 1986*a*). At the other extreme, even though unlike dislocations may be distributed randomly, the broadening is likely to be a mix between the Gaussian, which may dominate, some Cauchy, and shaping from the subgrain size parameters.

The results given in Table 3 allow a simple alternative explanation of differences observed between 'cold-worked' fragments and sputtered films. Although both may be prepared in highly imperfect states, one can explain the differences in terms of correlated dislocations. Filings show a high degree of clustering (small $R_c/\langle L\rangle$), while sputtered films show a broad distribution of dislocations (large $R_c/\langle L\rangle$). These differences can be related to sample conditions such as the temperature and local conditions at which the high-density dislocation structure is produced. Fragments produced by filing or grinding at room temperature may not be 'cold'. Instead, they may be rapidly heated to a high temperature during fracture, and rapidly quenched such that dislocations are mobile for short periods of time over short distances. On the other hand, sputtered films deposited onto an unlike substrate at or even somewhat above room temperature do not appear to have comparable dislocation mobility. Consequently, unlike dislocation pairs do not become highly correlated.

This research was sponsored by the Office of Naval Research Grant No. N00014-83-K-0750, P00004. The authors would like to express their thanks to Professor

M. A. Krivoglaz for his careful review of the manuscript.

References

AQUA, E. N. & WAGNER, C. N. J. (1964). *Philos. Mag.* **9**, 565-589.
DESPUJOLS, J. & WARREN, B. E. (1958). *J. Appl. Phys.* **29**, 195-199.
HOUSKA, C. R. & SMITH, T. (1981). *J. Appl. Phys.* **52**, 748-754.
KRIVOGLAZ, M. A., MARTYNENKO, O. V. & RYABOSHOPKA, K. P. (1983). *Phys. Met. Metall.* **55**, 1-12.
MCKEEHAN, M. & WARREN, B. E. (1953). *J. Appl. Phys.* **24**, 52-56.
RAO, S. & HOUSKA, C. R. (1986*a*). *Acta Cryst.* A**42**, 6-13.
RAO, S. & HOUSKA, C. R. (1986*b*). *Acta Cryst.* A**42**, 14-19.
WARREN, B. E. (1959). *Prog. Met. Phys.* Vol. VIII.
WILKENS. M. (1970). *Theoretical Aspects of Kinematical X-ray Diffraction Profiles from Crystals Containing Dislocation Distributions.* In *Fundamental Aspects of Dislocation Theory*, edited by J. A. SIMMONS, R. DEWIT & R. BULLOUGH. *Natl Bur. Stand. (U.S.) Spec. Publ.* No. 317, p. 11.

Acta Cryst. (1988). A**44**, 1028-1035

The Identification of Sb_5O_7I Polytypes from Optical Properties in the Ferroic Phase

BY I. R. JAHN, W. ALTENBURGER AND W. PRANDL

Institut für Kristallographie der Universität Tübingen, Charlottenstrasse 33, *D*-7400 *Tübingen, Federal Republic of Germany*

AND V. KRÄMER

Kristallographisches Institut der Universität Freiburg, Hebelstrasse 25, *D*-7800 *Freiburg, Federal Republic of Germany*

(*Received* 4 *January* 1988; *accepted* 1 *June* 1988)

Dedicated to Professor H. Dachs on the occasion of his 60th birthday

Abstract

The polytypic stacking sequences of Sb_5O_7I (SOI) which are possible up to a ten-module period are derived together with their most probable space groups. It is found that the driving force of the reversible structural phase transition occurring in all polytypes is systematically modified by the polytypic degree of freedom. By defining only three interlayer interactions - each realized in a pure way by a simple polytype - the transition temperature T_c of any stacking sequence can be predicted. The indicatrix orientation of SOI crystals depends on the proportion of + and − modules in a sequence. The extinction angle α is calculated on the basis of experimental data. The independent variables T_c and α are used for the identification of six higher polytypes of Sb_5O_7I.

1. Introduction

The determination of polytypic structures from bulk physical properties alone is restricted by severe conditions. The polytypic degree of freedom should influence several properties of a compound in a different manner. Of course, the effects would have to be measurable with a high accuracy in order to detect the tiny differences between long stacking sequences. Large samples without stacking faults are needed. In a few cases optical studies have proved to be useful. In ZnS polytypes, for example, the number of hexagonal stackings per identity period could be derived from the birefringence (Brafman & Steinberger, 1966).

Among all the polytypic structures antimony(III) oxide iodide, Sb_5O_7I (SOI), has a unique position (Nitsche, Krämer, Schuhmacher & Bussmann, 1977). Each modification undergoes a reversible structural phase transition which does not interfere with the polytypic degree of freedom itself. The polytypism, however, influences the properties of SOI fundamentally. This is indicated by the individual transition temperatures ($438 \leq T_c \leq 481$ K) of the eight polytypes distinguished so far and, more clearly, by the fact that some of them show pure ferroelasticity whereas others combine ferroelastic and ferroelectric behaviour in the low-symmetric phase. In principle, any ferroic property of SOI could be checked to see whether it contributes to the identification of the higher polytypes. The studies performed until now do not suffice for such an analysis.

This work was stimulated by the observation that the polytypic modifications of SOI differ in their crystal optics (Nitsche, Krämer, Schuhmacher & Bussmann, 1977). We analyse the differences in detail. It is demonstrated that Sb_5O_7I offers for the first time the chance to attack successfully the identification problem of a complex polytypic structure simply by measuring bulk physical properties of the system. We first describe the structure of SOI and discuss suitable

0108-7673/88/061028-08$03.00